Modeling the response of Greenland outlet glaciers to global warming using a coupled flowline-plume model

Johanna Beckmann[1], Mahé Perrette[1], Sebastian Beyer[1,2], Reinhard Calov[1], Matteo Willeit[1], and Andrey Ganopolski[1]

[1] Potsdam Institute for Climate Impact Research, 14412 Potsdam, Germany
[2] Alfred Wegner Institute, 27570 Bremerhaven, Germany

Correspondence: Johanna Beckmannn (beckmann@pik-potsdam.de)

Abstract.

In recent decades, the Greenland Ice Sheet has experienced an accelerated mass loss, contributing to approximately 25 % of contemporary sea level rise. This mass loss is caused by increased surface melt over a large area of the ice sheet and by the thinning, retreat and acceleration of numerous Greenland outlet glaciers. The latter is likely connected to enhanced submarine

5 melting that, in turn, can be explained by ocean warming and enhanced subglacial discharge. The mechanisms involved in submarine melting are not yet fully understood and are only crudely incorporated in some models of the Greenland Ice Sheet. Here, we investigate the response of twelve representative Greenland outlet glaciers to atmospheric and oceanic warming using a coupled 1D line-plume glacier-flowline model. The model parameters have been tuned for individual outlet glaciers using present-day observational constraints. We then run the model from present to the year 2100, forcing the model with

10 changes in surface mass balance and surface runoff from simulations with a regional climate model for the RCP 8.5 scenario, and applying a linear ocean temperature warming with different rates of changes representing uncertainties in the CMIP 5 model experiments for the same climate change scenario. We also used different initial temperature-salinity profiles obtained from direct measurements and from ocean reanalysis data. Using different combinations of submarine melting and calving parameters that reproduce the present-day state of the glaciers, we estimated uncertainties in the contribution to global sea

15 level rise for individual glaciers. We also performed a factor analysis, which shows that the role of different forcing (change in surface mass balance, ocean temperature and subglacial discharge) are diverse for individual glaciers. We found that changes in, ocean temperature and subglacial discharge are of comparable importance for the cumulative contribution of all twelve glaciers to global sea level rise in the 21st century. The median range of the cumulative contribution to the global sea level rise for all twelve glaciers is about 14 mm from which roughly 85 % are associated with the response to increased submarine

20 melting and the remaining part to surface mass loss. We also found a weak correlation (correlation coefficient 0.35) between present-day grounding line discharge and their future contribution to sea level rise in 2100. If the contribution of the twelve glaciers is scaled up to the total present-day discharge of Greenland, we estimate the contribution of all Greenland glaciers to 21st-century sea level rise to be approximately 50 mm. This result confirms earlier studies that the response of the outlet glaciers to global warming has to be taken into account to correctly assess the total contribution of Greenland to sea level

25 change.

1 Introduction

Sea level rise (SLR) is one of the major threats to humanity under global warming, and approximately one-fourth of the recent SLR can be attributed to the Greenland Ice Sheet (GrIS) (Chen et al., 2017). In the future projections of SLR, the GrIS is not only one of the major potential contributors but also a significant source of uncertainty. Two processes are largely responsible

5 for the GrIS contribution to SLR: (1) increased surface melt induced by global warming and (2) dynamic mass loss due to retreat and acceleration of outlet glaciers (Khan et al., 2014). The latter, which is most pronounced for marine- terminating outlet glaciers (Moon et al., 2012), is potentially caused by an increase in submarine melting, which can in turn be attributed to a warming of the ocean and increased subglacial discharge (Straneo and Heimbach, 2013). Regarding the first mechanism, the maximum contribution due to increased surface melt is estimated to range between 0 to 130 mm by the year 2100 (Fettweis

10 et al., 2013). Due to the possibility of applying relatively high-resolution regional climate models, confidence in this estimate has increased in the recent years (van den Broeke et al., 2017). The contribution of the second process remains highly uncertain because processes related to the response of marine-terminated Greenland glaciers are still not properly represented in the contemporary GrIS models (Straneo and Heimbach, 2013).

The principal objective of this paper is to quantify the response of marine-terminating outlet glaciers to future submarine

15 melting and to analyze whether the impacts of ice-ocean interaction on SLR are comparable to long-term changes in surface mass balance (SMB). In order to assess Greenland's contribution to future sea level rise, several different model strategies have been proposed. The most common method is to use three-dimensional ice sheet models, tuned to present-day conditions, and apply future climate change projections based on global or regional climate models. However, such models still have relatively coarse spatial resolution and cannot properly resolve most of the outlet glaciers that terminate in Greenland's fjords. They also

20 do not describe the interaction between glaciers and the ocean explicitly, but in some cases, for instance in Fürst et al. (2015), ocean melting is parameterized indirectly by increasing the basal sliding factor as ocean temperature increases. For the RCP scenario 8.5, they calculated a SLR between 155 and 166 mm at the year 2100 for the entire ice sheet atmospheric and oceanic forcing. Another method, followed by Nick et al. (2013), is to simulate single outlet glaciers individually using a 1-dimensional (1D) flowline model. Nick et al. (2013) performed simulations for four outlet glaciers that collectively drain about 22 % of

25 the total solid ice discharge of the Greenland Ice Sheet. Assuming proportionality between the future contribution to SLR and present-day ice discharge, Nick et al. (2013) scaled up results obtained from four glaciers to the total estimate of all Greenland outlet glaciers, which resulted in a range between 65 and 183 mm by the year 2100. Taking this one step further, Goelzer et al. (2013) used the results from Nick et al. (2013) in a 3D coarse-resolution ice sheet model. They applied the 1D glacier thinning and grounding-line retreat scenarios as an external, pre-calculated forcing in the grid cells at the ice sheet boundary.

30 Since only four glaciers had been simulated in the 1D model, they mapped the forcing from the original glaciers onto all other Greenland's marine-terminating outlet glaciers with a nearest neighbour approach. The incorporation added only 8 to 18 mm SLR on top of the stand-alone 3D ice sheet model simulation. Goelzer et al. (2013) argued that, that the smaller contribution results from smaller marine-terminating glacier that fully retreat in the 3D ice simulations, leaving no more ice-ocean , which is still included by the upscaling from Nick et al. (2013). Since we are especially interested in the impacts of ice-ocean interactions

on glacier dynamics, we followed an approach similar to Nick et al. (2013) but with several notable improvements. Firstly, for calculations of the vertically distributed submarine melt, we used a turbulent plume parameterization following Jenkins (2011). According to this parameterization, the submarine melt rate depends not only on ambient water temperature in fjords but also on seasonally varying subglacial discharge. The first idealized simulations of a coupled flowline-plume model were carried

5 out by Amundson and Carroll (2018) by using the maximum melt rate as a frontal ablation factor to account for undercutting plus calving of tidewater glaciers, demonstrating the potential impact of the subglacial discharge on glacier dynamics. For the evolution of the surface mass balance, we used anomalies computed by the regional climate model MAR and corrected them for elevation change. Finally, we performed simulations for 12 representative Greenland glaciers (compared to four in Nick et al. (2013)). This enabled us to test the assumption used in Nick et al. (2013) that the contribution of individual Greenland outlet

10 glaciers to SLR is proportional to their present-day discharge and therefore the total contribution of Greenland outlet glaciers can be obtained by scaling up contribution of individual glaciers proportionally to the entire present-day discharge of all outlet glaciers. We also estimated the uncertainties in the contribution of Greenland glaciers to SLR resulting from uncertainties in calving and ocean melt parameters and climate change scenarios.

The paper is structured as follows. First, we describe the coupled flowline-plume model, then how the input data were

15 preprocessed together with the experimental setting and climate change scenarios. Finally, we present the results of our model simulations for present day and future scenarios.

2   The coupled flowline-plume model

Most of Greenland's outlet glaciers terminate in fjords that are connected to the ocean. Inside these fjords, observations of upwelling plumes along the edges of glaciers have drawn attention to the importance of submarine melting. Consequently,

20 considerable efforts in modeling of submarine melt rate have been undertaken by using high-resolution 3D and 2D ocean general circulation models that are tuned to or parameterized after the buoyant-plume theory (Sciascia et al., 2013; Xu et al., 2013; Slater et al., 2015; Cowton et al., 2015; Carroll et al., 2015; Slater et al., 2017). However, such models are too computationally expensive and therefore impractical for simulating the response of the entire GrIS to climate change on centennial timescales. At the same time, recent studies demonstrate that the simple line plume model by Jenkins (2011) is an adequate tool to sim-

25 ulate plume behavior (Jackson et al., 2017) and to determine submarine melt rates for marine-terminated glaciers (Beckmann et al., 2018). Since the plume model is significantly less computationally expensive than 3D ocean models, it represents an alternative approach to introduce ice-ocean interaction into the GrIS model and still maintain the model's ability to perform a large set of centennial-scale experiments. Simulating the glacier dynamics with 3D ice sheet model requires very high spatial resolution ($\ll 1$ km) resulting in high computational cost (e. g. Aschwanden et al., 2016) and so far they cannot be used for

30 centennial timescales. To reduce the computational cost we used instead a 1D depth- and width- integrated one-dimensional ice flow model (Enderlin and Howat, 2013; Nick et al., 2013) coupled to a line plume model (Beckmann et al., 2018).

2.1 Glacier model

The governing equations of the 1D model include mass conservation:

$$\frac{\partial H}{\partial t} = -\frac{1}{W}\frac{\partial (UHW)}{\partial x} + B \tag{1}$$

where H is ice thickness, t is time, U is the vertically averaged horizontal ice velocity, W is the width and x is the distance

5 from the ice divide along the central flowline. B is the sum of SMB and submarine melting.

The conservation of momentum involves a balance between longitudinal stress, basal shear stress and lateral stress on the one hand, and driving stress on the other:

$$2\frac{\partial}{\partial x}\left(H\nu\frac{\partial U}{\partial x}\right) - A_s\left[(H - \frac{\rho_w}{\rho_i}D)U\right]^q - \frac{2H}{W}\left(\frac{5U}{EAWW_s}\right)^{\frac{1}{3}} = \rho_i g H\frac{\partial h_s}{\partial x}, \tag{2}$$

where h_s denotes the ice surface height, D the depth of glacier below sea-level, ρ_i and ρ_w the ice and sea water density,

10 respectively. Basal stress is parameterized with the basal sliding coefficient A_s and velocity exponent q and lateral stress involves a nondimensional width-scaling parameter W_s. Finally, the rate factor A and the enhancement factor E determine the viscosity ν

$$\nu = (EA)^{\frac{1}{3}}\left|\frac{\partial U}{\partial x}\right|^{-\frac{2}{3}}. \tag{3}$$

Calving occurs when surface crevasses propagate until the water level (Nick et al., 2013). Crevasses depth d_s is calculated

15 from the resistive stress $R_{xx} = 2\left(\frac{1}{A}\frac{\partial U}{\partial x}\right)^{1/3}$, as ice stretches, and can be enhanced by melt water depth d_w:

$$d_s = \frac{R_{xx}}{\rho_i g} + d_w\frac{\rho_0}{\rho_i} \tag{4}$$

where ρ_0 is the freshwater density.

Initial boundary condition is U(x=0) = 0, while at the calving front, we use

$$\frac{dU}{dx} = EA\left[\frac{\rho_i g H}{4}\left(1 - \frac{\rho_i}{\rho_w}\right)\right]^3 \tag{5}$$

20 The model employs a stretched horizontal grid with a horizontal resolution of 100 meters, where velocity is calculated at mid-points. At each time step of 3.65 days, the grid is stretched to keep track of the grounding line position, which is determined by the flotation criterion

$$H_{\text{float}} \le |z_b|\frac{\rho_w}{\rho_i}, \tag{6}$$

where z_b is the bedrock depth. Glacier thickness H and bedrock depth z_b of each cell interface are determined by linear

25 interpolation between the cell centered values.

The code is written is fortran, following the numerical procedure of Enderlin et al. (2013). The main differences compared to their original matlab code[1] is that we include a subgrid-scale treatment of the calving front boundary, and an improved treatment of the submarine melting.

---

[1]available at https://sites.google.com/site/ellynenderlin/research

2.2 Plume model

The plume model equations are described in Beckmann et al. (2018). We set the entrainment parameter E to 0.036, as suggested by Beckmann et al. (2018), Since the plume model in some cases underestimates and in others overestimates submarine melt rates (Beckmann et al., 2018), we also scale the simulated melt rate profile by a factor β, which we treat as a tuning parameter
5 within the range 0.3 - 3 (see section 4.1). The plume model employs a finer spatial resolution of < 1 m.

2.3 Coupling between glacier and plume model

Unlike Amundson and Carroll (2018), who used the maximum melt rate as a frontal ablation factor for tidewater glaciers, we take into account the entire vertical melt rate profile calculated with the plume model. Submarine melting volume flux is calculated for each cell and is applied as a vertical thinning rate on the floating tongue ($x_{g+1}...x_c$), or on the last grounded cell
10 (x_g) in the case of tidewater glaciers (no floating tongue). The melt rate m is integrated from the grounding line (position x_{gl}) along the bottom face of the floating tongue (if any), and along the calving face (position x_{cf}) up to sea level (Fig. 1), or to the top height of the risen plume (which can stop before sea level). The cumulative melt rate is given by

$$M = \int m(s)\, ds = \int_{x_{gl}}^{x_{cf}} m(h_b(x)) \cdot (\cos\alpha)^{-1} dx + \int_{h_b(x_{cf})}^{0} m(z) dz \qquad (7)$$

where s is the distance coordinate along the tongue bottom and the vertical calving face, h_b denotes bottom ice elevation, and
15 $cos\alpha$ is the variable tongue slope (calculated from the relation $\tan\alpha = \frac{\partial h_b}{\partial x}$). The integral is distributed over various cells (or only one cell (x_g) in the case of a tidewater glacier, where the first integral term is also zero since $x_{gl} = x_{cf}$), and the volume flux is added to the vertical mass balance term B, along with surface mass balance. Since the plume model does not allow for negative values of α, its minimum value is set to 10^{-6}. If the plume already ceases before reaching the calving front x_{cf}, we calculate a 2nd plume that starts at $h_b(x_cf)$ with the initial minimum default discharge value of $10^{-6} m^3 s^{-1}$ to assure a
20 background frontal melting.

Subglacial discharge Q was computed off-line using the ice sheet model with explicit treatment of basal hydrology (Section 3.3), then applied to the line plume in distributed form $q = Q(W)^{-1}$. It is assumed that plume properties (velocity, temperature, salinity, and thickness) in the coupled model adapt instantaneously to changes in the glacier's shape, subglacial discharge, temperature and salinity profiles of ambient water. The glacier and plume model exchange information at every time step of
25 the glacier model.

3 Model Input

3.1 The choice of glaciers

In this study, we modeled twelve, well-studied Greenland outlet glaciers of different sizes and located in different regions of Greenland (Fig. 2). One criterion of this selection is that the glaciers should represent different types of ice flows and

different environmental conditions. Also, did we include small marine-terminating glaciers to assure a more realistic upscaling as Goelzer et al. (2013) indicates. Besides that, for most of the chosen glaciers, Enderlin and Howat (2013) estimated melting to calving ratio which we use as an additional constraint on the choice of modeling parameters.

3.2 Glacier geometry

5 For each individual glacier, bedrock elevation and width were determined by analyzing cross-sections taken at regular intervals along the glacier flow, generally covering a large portion of the glacier catchment area (Perrette et al., in prep). In each cross-section, the procedure comes down to calculating a flux-weighted average for bedrock elevation, ice velocity U and thickness H, and choose the glacier width W such that the flux F through the cross-section is conserved, i.e. $W = F/(UH)$ (Perrette et al., in prep). We use the BedmACHInev2 data for bedrock topography (Morlighem et al., 2014). Fjord bathymetry was extended
10 manually by considering available data (Mortensen et al., 2013; Schaffer et al., 2016; Dowdeswell et al., 2010; Syvitski et al., 1996; Rignot et al., 2016). For ice velocity we use data from Rignot and Mouginot (2012). The resulting glacier profiles are depicted in Fig. 9.

3.3 Subglacial discharge and glacier surface mass balance

To force the plume model, we use monthly averaged subglacial discharge. Subglacial discharge represents the sum of basal
15 melt, water drainage from the temperate layer and surface runoff. The former two sources are computed directly in the ice sheet model (Calov et al. 2018). In reality surface runoff can travel along the ice surface until it either reaches an existing connection to the bedrock (e.g. crack) or it accumulates in a supraglacial lake that eventually drains, making a new connection. However, these processes are too complex and still poorly understood. This is why in our relatively coarse (5 km) resolution ice sheet model (Calov et al., 2018), we neglect these short scale processes and assume that runoff penetrates directly down to
20 the bedrock. The surface runoff and SMB anomalies for present day and future scenarios are taken from experiments with the regional climate model MAR (Fettweis et al., 2013) and corrected for the future surface elevation change (Calov et al., 2018). The entire water (runoff, basal melt, and water from the temperate layer) is routed by the hydraulic potential using a multi-flow direction flux routing algorithm, as described in (Calov et al., 2018). All water transfer is assumed to be instantaneous. Water that passes the grounding line (defined by the ice mask from SICOPOLIS) is assigned to the closest glacier within a maximum
25 distance of 50 km.

In our future scenarios when simulating subglacial discharge we account for changes in surface runoff, basal melt, and ice sheet elevation but neglect the effect of grounding line retreat. This means that we route the subglacial discharge always to the present-day position of the grounding line.

In this study, we use a single scenario for future surface runoff and SMB change, namely, a simulation with the regional
30 model MAR nested in the global GCM MIROC5 model forced by the RCP 8.5 scenario. Among the CMIP5 models, MIROC5 simulate climate change which leads to a medium contribution of GrIS to future SLR (Calov et al., 2018). To correct for possible model biases in the future scenarios for surface runoff and SMB, we added the simulated MIROC5 anomalies to the reference climatology simulated for the same period with the MAR model forced by ERA reanalysis data. We also corrected

model surface runoff and SMB for changes in surface elevation by applying the gradient method of Helsen et al. (2012) as described in Calov et al. (2018). The surface runoff R over the ice sheet (SICOPOLIS) is determined as

$$
\begin{aligned}
R(x,y,t) = R_{\mathrm{MAR(REAN)}}^{\mathrm{Clim\ 1961-1990}}(x,y) \quad &+ \quad (R_{\mathrm{MAR(MIROC)}}(x,y,t) - R_{\mathrm{MAR(MIROC)}}^{\mathrm{Clim\ 1961-1990}}(x,y)) \\
&+ \quad \left(\frac{\partial R}{\partial z}\right)_{\mathrm{MAR(MIROC)}}(x,y,t) \quad \Delta h_s(x,y,t),
\end{aligned}
\tag{8}
$$

where the runoff $R(x,y,t)$ on every grid cell (x,y) at any time t is calculated by the climatological mean from 1961-1990 of MAR (forced by reanalysis data) $R_{\mathrm{MAR(rean)}}^{\mathrm{Clim\ 1961-1990}}(x,y)$ plus the anomaly of the runoff relative to the climatological mean for the same period of time obtained by MAR forced with MIROC5 $(R_{\mathrm{MAR(CMIP5)}}(x,y,t) - R_{\mathrm{MAR(CMIP5)}}^{\mathrm{Clim\ 1961-1990}}(x,y))$. For ice surface evolving in time $\Delta h_s(x,y,t) = h_s^{\mathrm{obs}}(x,y) - h_s(x,y,t)$, the vertical gradient $\left(\frac{\partial R}{\partial z}\right)_{\mathrm{MAR(MIROC)}}(x,y,t)$ determined for every time step, is additionally applied to accounting for the increase in surface runoff. The observed surface elevation h_s^{obs} of the ice sheet is taken from Bamber et al. (2013). Negative runoff values are set to zero. The correction of runoff for elevation change can be important in some case since as it was shown in Amundson and Carroll (2018), for tidewater glaciers, large and rapid changes in glacier volume can lead to a high increase in runoff due to surface lowering.

For the present-day condition, SMB is calculated from relaxation to observed surface elevation h_s^{obs}, with a different relaxation time scale τ for each glacier (see section 4.1):

$$
\mathrm{SMB} = \frac{h_s^{\mathrm{obs}} - h_s}{\tau} \ \ \text{in m/yr.}
\tag{9}
$$

We refer to this flux as implied SMB, calculated during the spinup experiment. For future scenarios, we added the anomaly of the SMB (relative to the year 2000) to the implied SMB. The anomaly for each grid cell of the glacier was computed from interpolation of the MAR anomaly of the centerline of the individual glacier and additionally corrected for the glacier elevation change similarly to the surface runoff (Eq. 8), but for the SMB-calculation, Δh_s is the glacier elevation change compared to present-day, assuming that the derived glacier shape from the present-day dataset is for the year 2000. The time series of cumulative SMB (without surface correction) and the annual subglacial discharge for each glacier are shown in the supporting information (Fig. S1 and Fig. S2)

3.4 Fjord temperature and salinity profiles: CTD measurement and Ocean Reanalysis data

Determining vertical temperature and salinity profiles, which are the input for the plume model, is a challenging task. Measurements inside Greenland fjords are rare and do not cover all of them. For some fjords, several conductivity-temperature-depth (CTD) measurements exist, but they are mostly infrequent and often not performed close enough to the calving front. Hence, the question arises on how to treat fjords, where no CTD measurements are available. A possible solution is to use ocean reanalysis data. Here we use the TOPAZ Arctic Ocean Reanalysis data[2] (Xie et al., 2017) and compare them with existing CTD measurements as well as analyze potential impact of the differences between reanalysis and CTD profiles on the glacier

---

[2]http://marine.copernicus.eu/services-portfolio/access-to-products/?option=com_csw&view=details&product_id=ARCTIC_REANALYSIS_PHYS_002_003

response to climate change. The TOPAZ dataset was produced with the ocean model HYCOM using in situ measurements and satellite data sets. It covers the time span from 1991–2013 with a spatial resolution of 12.5 km. Below 200 m depth an error $> 1°C$ and > 0.1 psu can occur. The dataset does not resolve the Greenland fjords and covers only the open ocean and continental shelf. It is known that the vertical T-S profile inside the fjords can resemble the profile in the open sea (Straneo

5   et al., 2012; Straneo and Heimbach, 2013; Inall et al., 2014). However, often a grid cell in the ocean reanalysis data can be located hundreds of km from the fjord mouth, where other ocean conditions might prevail.

Figure 3 illustrates this problem for the Kangerlussuaq glacier: much colder temperatures are measured by CTDs at depths below 400 m inside of the fjord compare to the measurements at the same depths but far outside of the fjord. A calculation with the line plume shows that the melt rate with the mid-fjord CTD (white dot, and dashed line at ~ 210 km distance in panel

10   b) would increase by 80 % when melt rate is calculated using the outermost CTD (white dot, at   400 km distance) for a typical subglacial summer discharge. Furthermore, the presence of sill(s) in the fjord and fjord circulation can affect significantly the T-S profile in the vicinity of the glacier front.

It is also important to note that T-S profiles obtained from CTD measurements have to be treated with caution because they represent only a 'time shot' of fjord properties which vary in time significantly (Jackson et al., 2014). Due to all these

15   uncertainties, here we test how sensitive the model response is to the chosen present-day T-S profile when carrying out future climate change simulations (Section 5). To this aim, we first compared temperature-salinity profiles of the reanalysis data to available CTD measurements inside the fjords made as close as possible to the glacier fronts. We constructed the T-S profiles from the reanalysis dataset by detecting the closest grid-cell to the fjord mouth. For comparison, we used the reanalysis data at depth 200, 400 and 700 meters, since they represent typical depths of Greenland fjords and glacier grounding lines.

20   Figure 4 and 5 compare the temperature at these depths from reanalysis data with available CTD profiles measured over past several decades. Since Greenland is surrounded by the continental shelf with typical depths of 200-400 meters, most of the 700-meter depth points in reanalysis data are located outside the fjords in the deeper ocean, far away from the glacier mouth as shown in Fig. 6 for Store Glacier. For the Store Glacier, the temperature at 700m depth inside the fjord measured by CTD is much warmer than the temperature in reanalysis data at the same depth, which can potentially be explained by the

25   shallow continental shelf. As Schaffer et al. (2017) showed, for the Nioghalvfjerdsfjorden Glacier, the continental shelf works similarly to a sill that blocks waters of greater depths and favors water masses above the shelf to pass into the fjord. For all of the investigated glaciers, we found better matching profiles of reanalysis to CTD profiles if we neglected the reanalysis temperature of 700m-depth locations (mostly outside continental shelf) and used instead the 400m-depth temperature (mainly on the continental shelf) for all depths below 400 m. If the grounding line depth was larger than 400 m, temperatures below that

30   depth were assumed to be equal to the temperature at 400m- depth in the reanalysis data. The corresponding salinity profile at the same 400m-depth data point was equally modulated as the temperature profile. The location of the reanalysis data point is listed in Table 1 of the supporting information.

To produce a "present-day" T-S profile that resembles inside-fjord conditions, we averaged temperature and salinity from reanalysis data over period 1990-2010 in the grid cell closest to corresponding fjord mouth and with a depth of at least 400 m.

If the fjord does not have 'blocking' sills, we extrapolate the water properties at 400m depth down to depths of the grounding lines as described above. For these investigated glaciers, we found no sills shallower than the 400m depth in the data set.

These T-S profiles constructed from the reanalysis data, as well as those from the CTD measurements, were used as the boundary conditions in the plume model. Figure 7 shows that the vertically averaged temperatures derived from reanalysis data are colder than those from CTD measurements for most of the selected glaciers. This bias also remains when choosing reanalysis temperature for the same periods when the CTD measurements were taken (not shown). In the following section, we investigate how these biases may affect glacier response to future climate change.

For the simulations of the future, we prescribed simple scenarios for the ocean temperature anomalies based on temperature trends simulated by several CMIP5 models (GFDL-ESM2G, MPI-ESM-LR, and HadGEM2-CC). We use again the closest 400m-depth-point neighbor of each CMIP5 model dataset to the fjord mouth. From this model cell, the temperature trend is derived with linear regression as illustrated in Fig. 8. The trend and cell location for each glacier and CMIP5 model are listed in Table S1 of the supporting information, while the resulting minimal and maximal temperature trend for each glacier is listed in Table 1.

4 Experimental setup

4.1 Selection of model parameters and model spin up

First, the stand alone glacier model (without the plume parameterization) was pre-calibrated to reproduce observed surface elevation, grounding-line position and velocity profile assuming a constant prescribed submarine melt rate. Dynamic parameters E, W_s, A_s and q were varied for this purpose (affecting basal shear stress, lateral stress, and calving front boundary condition), along with the freshwater depth in crevasses d_w and the constant melt rate m, for each glacier separately. For most glaciers we use 20 or 30 years for the surface relaxation time scale τ for SMB (Eq. 9), but for some glaciers (e.g. Daugaard-Jensen) τ was set to 100 years.

Once the four dynamic parameters and the relaxation time scale are set, we switch to the coupled glacier-plume model. For the spinup experiments, we used monthly subglacial discharge for the year 2000. Vertical temperature and salinity profiles in these experiments were taken from recent CTD data or reanalysis data, averaged over the time interval 1990-2010, and held constant. Thus, the only factors affecting submarine melt profile in spin-up experiments are the depth of grounding line and the shape of the floating tongue (if present).

We generate an ensemble by varying freshwater depth in crevasses d_w and the plume scaling parameter β (in a range from 0.3 to 3), which control calving and submarine melting, respectively. We run the coupled model for each combination over 100 years, so that the glacier is close to an equilibrium state and we exclude model versions whose grounding line is further than 2 km from the observed grounding line, as diagnosed from the 1D profile, or which displays a low-frequency oscillatory behaviour with advancing glacier front over the last 20 years. For the glaciers for which partition between calving and submarine melting was available from Enderlin and Howat (2013), we used this partition as an additional constraint for the model parameter combinations.

4.2 Future climate scenarios

For all future simulations, we used valid combinations of model parameters and corresponding initial conditions obtained at the end of 100-yrs spin-up runs. The anomalies of SMB were derived from the regional climate model MAR simulations as described in Section 3.3 (Fig. S1). To compute the submarine melt rate, we use the minimal and maximal ocean temperature

5   trends for each glacier 3.4 listed in Table 1 (Section 3.4). The subglacial discharge was prescribed on a monthly time step with the derived subglacial discharge data from SICOPOLIS (Calov et al., 2018) for each glacier individually 3.3 (yearly values depicted in Fig. S2).

All forcing scenarios were applied for the years $2000 - 2100$. In addition, we run the model for 100 years with zero anomalies of temperature, SMB, and subglacial discharge to determine unforced model drift.

10   To express ice volume loss in sea level rise equivalent we used the multiplication factor t under the assumption of oceans occupying $A_{\mathrm{ocean}} = 360 \cdot 10^6 \ \mathrm{km}^2$:

$$t = \frac{\rho_{\mathrm{ice}}}{\rho_{\mathrm{fw}} A_{\mathrm{ocean}}} \tag{10}$$

leads to a SLR of $2.55 \cdot 10^{-3}$ mm for $1 \ \mathrm{km}^3$ of ice volume V_{SLR}.

The contributing ice volume V_{SLR} is calculated with the total glacier volume V_{glacier} subtracted by the floating ice volume

15   V_{fl}, ice volume under sea level V_{uSL} and the additional 12 % that - if melted- would not contribute to SLR, since the created ice-free space would be filled up by sea water (bedrock to sea level). Thus, the ice volume that only contributes to SLR is

$$V_{\mathrm{SLR}} = V_{\mathrm{glacier}} - V_{fl} - V_{\mathrm{uSL}} \ \frac{\rho_{\mathrm{sw}}}{\rho_{\mathrm{ice}}}, \tag{11}$$

with the density of ice $\rho_{\mathrm{ice}} = 917 \ \mathrm{kg \ m^{-3}}$, sea water $\rho_{\mathrm{sw}} = 1028 \ \mathrm{kg \ m^{-3}}$ and fresh water $\rho_{\mathrm{fw}} = 1000 \ \mathrm{kg \ m^{-3}}$.

5 Results

20   ## 5.1 Present-day state

The simulated glacier thickness and velocity profiles for the different submarine melting and calving ratios are depicted in Fig. 9. We found that for some glaciers the grounding line demonstrates a high sensitivity to the melting/calving ratio, while others are primarily controlled by their bedrock topography and have relatively small changes in their grounding line position over the whole melting/calving- range. The Gade and Upernavik North glaciers are, for example, representative of the latter case (Fig.

25   S3). The simulated velocity profiles (Fig. 9) for Gade Glacier and Jakobshavn-Isbrae required a slightly thinner glacier than derived by the geometry of the dataset. We were only able to achieve stable states for Jakobshavn-Isbrae with the reanalysis dataset, since CTD measurements showed significantly warmer temperatures, and the resulting higher submarine melt rate in our simulations would lead to the retreat of the glacier on the retrograde bedrock.

Table 2 provides a comparison to observational data derived by Enderlin and Howat (2013). Only the glaciers Kong-Oscar

30   and Docker-Smith showed a grounding line flux $\mathrm{Flx}_{\mathrm{gl}}$ matching the observational data. All other glaciers have smaller grounding line fluxes than in Enderlin and Howat (2013). However, it should be noted that many glaciers accelerated since 2000, so it

is not clear whether the fluxes reported by Enderlin and Howat (2013) are true equilibrium fluxes. Additionally, Enderlin and Howat (2013) derived submarine melt rates for the floating termini of the glaciers. Note that Enderlin and Howat (2013) could not account for vertical glacier fronts due to their methodological approach. For a direct comparison to Enderlin and Howat (2013), we calculate $\mathrm{MeltFlx}$ of the simulated glaciers by only considering the mass loss from the floating tongue induced by

5 submarine melting. The ratios of submarine melting to grounding line discharge of our simulations lie within the uncertainty ranges determined byEnderlin and Howat (2013). However, these uncertainties are quite large and thus allow broad parameter combinations for some glaciers. For Jakobshavn, a high calving flux was needed in order for the coupled glacier-plume model to obtain similar velocities as the present-day velocity profile (Fig. 9) derived from the dataset. This resulted in calibrated glacier profiles without any floating terminus (and a numerical $\mathrm{MeltFlx} = 0.$), which was not observed by Enderlin and Howat

10 (2013). Thereafter, this simulated glacier does not match the ratio of submarine melting to grounding line discharge ratio determined by Enderlin and Howat (2013) ($\mathrm{MeltFlx}^{\star E}/\mathrm{Flx}_{\mathrm{gl}}^{\star E}$ Table 2). The high calving flux required in order to obtain the precise grounding line position might result from inconsistency with bedrock data or an information loss received by the flux-weighted averaging.

5.2 Future simulations

15 After obtaining the present-day state, we then ran all valid model versions for 100 simulation years, applying MAR SMB anomalies, monthly subglacial discharge and two scenarios for ocean temperature change (minimum and maximum) as forcing. All results shown here have the model drift subtracted from the calculated values. The glaciers' response to climate change strongly depends on the combination of model parameters and scenarios, resulting in high uncertainty ranges. The simulations that led to a median-range[3] SLR for each glacier is depicted in Figure 10. After 100 years, some glaciers retreat entirely and

20 become land-terminated (Alison, Daugaard-Jensen, Kangerlussuaq, Store), while others barely show a change in the position of the grounding line (Helheim). The individual contribution of each glacier to SLR for the median-range[3] SLR experiments is shown in Fig. 11 a. Jakobshavn-Isbrae shows the most significant contribution to SLR, due to the big catchment area and large retreat, followed by Kangerlussuaq Glacier due to its full retreat.

These median-range SLR experiments where forced by changes in SMB with the surface elevation feedback, ocean warming

25 T and increased subglacial discharge Q. Together, all 12 glaciers add up to almost 14 mm SLR at the year 2100. To quantify the individual tole of the forcing factors, the same model-experiments of the mid-range simulations were run excluding the different forcing factors. We found that from the 14 mm over 80 % of SLR is caused by increased submarine melting due to the additional ocean warming T and increased subglacial discharge Q (Fig. 11 b). Thereby both factors,(T and Q), contributed an equally high amount in SLR. The reaming 15 % of the 14mm SLR are attributed to the glacier's response to changes in

30 SMB (Fig. 11 b, orange courve). This is quite substantially ,considering the fact that the SMB-forcing alone derived from MAR (without the glacier's response) has an almost negligible effect on SLR (Fig. 11 b, brown curve). For some glaciers, the cumulative SMB (SLR ignoring glacier response) is even increasing towards the end of this century (Fig S1). The increased mass loss by glacier dynamics origins if surface mass loss is concentrated at the glacier terminus, resulting in thinning and

---

[3]median for an odd number of simulations, the first value of higher half for an even number of simulation

potentially triggering glacier retreat. Whether this, anyhow minor SMB forcing (brown curve) is corrected for surface elevation feedback (see Section 3.3) or not, is of no significance in respect to SLR (Fig. 11 b, orange and yellow curve).

These estimates of the role of separate factors (changes in SMB, ocean temperature and subglacial discharge) are, however, the result of the cumulative SLR of all glaciers. Each individual glacier may respond differently to the single forcing factor. For

5 instance, the Kong-Oscar Glacier (Fig. 12) is slightly gaining mass with the SMB forcing and shows a retreat by 10 km and contribution 1 mm to SLR only due to ocean warming. When the increase in subglacial discharge is considered additionally to the same ocean warming, the glacier retreats another 10 km and contributes to approximately 3 mm of SLR.

At the same time, the Yngvar-Nielson Glacier (Fig. 12) is already retreating significantly in the experiment with the SMB forcing alone. Ocean warming and increased subglacial discharge also contribute to SLR, but for Yngvar-Nielson the largest

10 SLR contributor is the SMB change. Above we discussed only median-range scenarios, but the uncertainty ranges are crucial when predicting SLR. Therefore, Fig. 14 shows the first and third quartile together with the median values of the individual glacier's contributions to SLR for all sets of valid model realizations and full forcing (SMB + T (max/min) + Q) against the simulated present-day discharge. Their potential SLR and grounding line retreat are listed in Table 3 and 4. Figure 14 shows a correlation between present-day grounding line discharge and the contribution to future SLR. Jakobshaven and Kong-Oscar

15 show the largest uncertainties. We investigate whether the uncertainty range results from the range of temperature forcing ($T_{\min}$ /$T_{\max}$) or model parameters by distinguishing for experiments with ($T_{\min}$ /$T_{\max}$) in Fig. 15. Figure 15 a shows that future SLR and its uncertainty related to SMB forcing alone are rather small (except for Jakobshaven-Isbrae). For glaciers like Daugaard-Jensen and Kong-Oscar, the negative SLR originates from the increase in SMB in this region under the RCP 8.5 scenario. Including the forcing factors of submarine melt, T and Q, leads to a relatively high SLR contribution and a high

20 SLR uncertainty range for the Kong-Oscar, Kangerlussuaq, Rink, and Daugaard-Jensen glaciers, Fig. 15 shown by the blue columns. Since these high uncertainties arise also with the same forcing (only $T_{\min}$ or $T_{\max}$), we attribute the major source of uncertainty to the different combinations of the model parameters d_w and β. For each experiment, we also investigated whether the choice of using CTD measurements or reanalysis data for the initial ocean temperature profile had an impact on the potential SLR. For the difference in SLR, we could only detect a slight increase when using reanalysis data instead of CTD

25 data for a few glaciers (Fig. S4)

In spite of these uncertainties, we use the median scenarios from Fig. 14 to estimate the relationship between present-day glacial discharge and contribution to SLR for the year 2100 by fitting a linear function determined with the least square method. The derived slope ($0.1 \, \mathrm{mm \, km^{-3} \, a}$) has weak correlation (correlation coefficient 0.35). With this slope and the total flux of all outlet glaciers ($\sim 450 \, \mathrm{Gt/a}$ (Enderlin et al., 2014; Rignot et al., 2008)), the simple linear relationship would imply a total

30 SLR contribution of roughly 5 cm from all Greenland outlet glaciers.

6 Discussion and Conclusions

For 12 individual outlet glaciers of the GrIS, we investigated their potential contribution to SLR during the 21st century for the RCP 8.5 scenario. To study the role of future changes in SMB, ocean temperature and subglacial discharge, we used a

1D flowline model with a surface crevasse calving law coupled to a 1D line plume model Jenkins (2011). In our model, the calving flux can be altered by choosing a parameter for the melt water depth in crevasses, and the submarine melt rate can be changed by a scaling factor. We also used two different initial temperature-salinity profiles – one derived from reanalysis data and another from in-situ measurements inside the fjords. For the present-day simulations, we varied the submarine melting

5   and the calving parameter to obtain a glacier profile similar to observations. For all outlet glaciers, we were able to achieve a reasonable agreement between the simulated and observed present-day profiles. However, for the Jakobshavn Isbrae glacier, the simulated submarine melt and grounding line discharge ratio does not agree with that derived by Enderlin and Howat (2013), as this ice stream could not develop a floating terminus in our simulations.

In order to simulate the future glacial contribution to SLR under the RCP 8.5 scenario, we prescribed changes in SMB and
10   subglacial discharge based on results of the regional climate model MAR. Anomalies of near-fjord ocean temperatures from CMIP5 global climate models served to generate minimum and maximum scenarios for the ocean temperature until year 2100. Simulated SLR contributions for the year 2100 compare well to values from Nick et al. (2013) for Jakobshavn Isbrae. The Kangerlussuaq Glacier exceeds the SLR estimation of Nick et al. by 2 mm, while for the Helheim Glacier our SLR estimations are below the estimations of Nick et al. (2013). The difference to Nick et al. (2013) can be explained by their different treatment
15   of future calving fluxes (freshwater depth was linked to future runoff) or submarine melting (excluding subglacial discharge). Also, Nick et al. (2013) used the surface elevation and velocity profile from the center line and took the width as the whole catchment area, whereas at Jakobshaven Isbrae, the width was constrained to the width of the trough and the lateral flux was added. By contrast, we use a flux-weighted average of the whole glacier catchment area to represent each individual glacier.

we use a flux-weighted average of the whole glacier catchment area, whereas Nick et al. (2013) used for e.g. Jakobshaven
20   Subrea a narrow channel and added lateral flow.

We also investigated how various forcing factors influence the simulated future SLR. For the ensemble of the 12 glaciers, SLR is sevenfold larger when the changes in subglacial discharge and ocean temperature were added to changes in SMB. This underlines the critical role of oceanic warming for future GrIS contribution to SLR. Moreover, we found significantly larger SLR when the subglacial discharge is allowed to increase in the scenarios. In fact, the amount of SLR attributed to subglacial
25   discharge is similar to the SLR attributed to an increased ocean temperature. Thus, for future projections, both factors affecting submarine melt rate – subglacial discharge and ocean temperature – need to be taken into account. It should also be noted that our 1D flowline model is based on a crevasse depth calving law and thus does not account for undercut calving or buoyancy-driven calving (Benn et al., 2017), which in turn is strongly influenced by submarine melting. This mechanism might act as a further amplifier of glacial mass loss that is not reflected in our results.

30   Our experiments also reveal large uncertainty ranges, primarily attributed to the different combinations of the two model parameters that determine submarine melting and calving fluxes. Nonetheless, the simulated melt/calving ratios lie within the uncertainty range of observations, and reducing the uncertainties with more precise observational data would probably improve future simulations. On the other hand, our results were not significantly affected by the choice of CTD or reanalysis data when defining the initial ocean temperature and salinity profile. This suggests that accurate process-based models and observational
35   constraints on submarine melt and calving are more important when making projections about future retreat of Greenland

outlet glaciers. Additional uncertainty related to dynamic parameters and topography data (bedrock, width) are not included in this study.

Overall, we obtain a total Greenland glaciers SLR contribution of approximately 5 cm when assuming a linear relationship between the glacier's present-day grounding line discharge and and future sea level rise. Our result is lower than the estimate in Nick et al. (2013) (6.5-18.3cm) due to the fact that we included smaller marine-terminating glaciers. As Goelzer et al. (2013) argues, these glaciers probably become land-terminating faster than glaciers with a large grounding line discharge and have less mass influenced by ice-ocean interaction. Therefore we think that our our upscaling method for this emissions scenario should not be used past the year 2100. Our simulations considered a constant catchment area for each glacier and did not account for potential lateral inflow from the ice sheet interior. Such increased mass inflow could result in a smaller grounding line retreat and thus decrease our SLR contribution estimate. However, an increased inflow would also result in a broadening of the catchment area, as Goelzer et al. (2013) indicate, which could increase mass loss further upstream. The full impact can only be assessed with experiments in which outlet glaciers and the parent ice sheet are fully coupled. For a first approximation, though, we treat the SLR of 5 cm as additional to that simulated with coarse resolution GrIS ice-sheet models, since the cumulative SMB forcing (without glacier response) over the glaciers' area is negligible. By adding the 5 cm contribution of outlet glaciers to the 8.8 cm simulated by Calov et al. (2018) for the year 2100 using the same climate scenario, we arrive at a total GrIS contribution 13.8 cm. This implies that the dynamical response of Greenland's outlet glaciers to global warming can increase GrIS contribution to SLR by over 50 %.

Author contributions.   J.B designed the study together with A. G.. M.P. developed the glacier model. J.B. coupled the numerical plume model to the glacier model, and implemented the surface-correction method. Together with S.B, R.C and M.W, J.B. created the projected subglacial discharge and surface-mass balance data set for each glacier respectively. J.B. carried out the experiments, created figures and wrote the manuscript, supported by all co-authors.

Competing interests.   The authors declare no competing interests.

Acknowledgements.   This work was funded by Leibniz-Gemeinschaft, WGL Pakt für Forschung SAW-2014-PIK-1. R. C. is funded by the Bundesministerium für Bildung und Forschung (BMBF) grants PalMod-1.1 and PalMod-1.3.

References

Amundson, J. M. and Carroll, D.: Effect of Topography on Subglacial Discharge and Submarine Melting During Tidewater Glacier Retreat, Journal of Geophysical Research: Earth Surface, 123, 66–79, https://doi.org/10.1002/2017JF004376, http://doi.wiley.com/10.1002/2017JF004376, 2018.

5 Aschwanden, A., Fahnestock, M. A., and Truffer, M.: Complex Greenland outlet glacier flow captured, Nature Communications, 7, 10 524, 2016.

Bamber, J. L., Griggs, J. a., Hurkmans, R. T. W. L., Dowdeswell, J. a., Gogineni, S. P., Howat, I., Mouginot, J., Paden, J., Palmer, S., Rignot, E., and Steinhage, D.: A new bed elevation dataset for Greenland, Cryosphere, 7, 499–510, https://doi.org/10.5194/tc-7-499-2013, 2013.

Beckmann, J., Perrette, M., and Ganopolski, A.: Simple models for the simulation of submarine melt for a Greenland glacial system model,
10 Cryosphere, 12, 301–323, https://doi.org/10.5194/tc-12-301-2018, 2018.

Benn, D. I., Aström, J., Zwinger, T., Todd, J., Nick, F. M., Cook, S., Hulton, N. R., and Luckman, A.: Melt-under-cutting and buoyancy-driven calving from tidewater glaciers: New insights from discrete element and continuum model simulations, Journal of Glaciology, 63, 691–702, https://doi.org/10.1017/jog.2017.41, 2017.

Calov, R., Beyer, S., Greve, R., Beckmann, J., Willeit, M., Kleiner, T., Rückamp, M., Humbert, A., and Ganopolski, A.: Simula-
15 tion of the future sea level contribution of Greenland with a new glacial system model, The Cryosphere Discussions, 2018, 1–37, https://doi.org/10.5194/tc-2018-23, https://www.the-cryosphere-discuss.net/tc-2018-23/, 2018.

Carroll, D., Sutherland, D. a., Shroyer, E. L., Nash, J. D., Catania, G. a., and Stearns, L. a.: Modeling Turbulent Subglacial Meltwater Plumes: Implications for Fjord-Scale Buoyancy-Driven Circulation, Journal of Physical Oceanography, p. In press, https://doi.org/10.1175/JPO-D-15-0033.1, http://journals.ametsoc.org/doi/abs/10.1175/JPO-D-15-0033.1, 2015.

20 Chen, X., Zhang, X., Church, J. A., Watson, C. S., King, M. A., Monselesan, D., Legresy, B., and Harig, C.: The increasing rate of global mean sea-level rise during 1993-2014, Nature Climate Change, 7, 492–495, https://doi.org/10.1038/nclimate3325, http://dx.doi.org/10.1038/nclimate3325{%}0Ahttp://10.0.4.14/nclimate3325{%}0Ahttp://www.nature.com/nclimate/journal/vaop/ncurrent/abs/nclimate3325.html{#}supplementary-information{%}5Cnhttp://www.nature.com/doifinder/10.1038/nclimate3325, 2017.

Cowton, T., Slater, D., Sole, A., Goldberg, D., and Nienow, P.: Modeling the impact of glacial runoff on fjord circulation and subma-
25 rine melt rate using a new subgrid-scale parameterization for glacial plumes, Journal of Geophysical Research: Oceans, 120, 796–812, https://doi.org/10.1002/2014JC010324, 2015.

Dowdeswell, J. A., Evans, J., and Cofaigh, C. Ó.: Submarine landforms and shallow acoustic stratigraphy of a 400 km-long fjord-shelf-slope transect, Kangerlussuaq margin, East Greenland, Quaternary Science Reviews, 29, 3359–3369, https://doi.org/10.1016/j.quascirev.2010.06.006, http://dx.doi.org/10.1016/j.quascirev.2010.06.006, 2010.

30 Enderlin, E. M. and Howat, I. M.: Submarine melt rate estimates for floating termini of Greenland outlet glaciers (2000–2010), Journal of Glaciology, 59, 67–75, https://doi.org/10.3189/2013JoG12J049, http://openurl.ingenta.com/content/xref?genre=article{&}issn=0022-1430{&}volume=59{&}issue=213{&}spage=67, 2013.

Enderlin, E. M., Howat, I. M., and Vieli, A.: High sensitivity of tidewater outlet glacier dynamics to shape, The Cryosphere, 7, 1007–1015, https://doi.org/10.5194/tc-7-1007-2013, http://www.the-cryosphere.net/7/1007/2013/, 2013.

35 Enderlin, E. M., Howat, I. M., Jeong, S., Noh, M. J., Van Angelen, J. H., and Van Den Broeke, M. R.: An improved mass budget for the Greenland ice sheet, Geophysical Research Letters, 41, 866–872, https://doi.org/10.1002/2013GL059010, 2014.

Fettweis, X., Franco, B., Tedesco, M., Van Angelen, J. H., Lenaerts, J. T., Van Den Broeke, M. R., and Gallée, H.: Estimating the Greenland ice sheet surface mass balance contribution to future sea level rise using the regional atmospheric climate model MAR, Cryosphere, 7, 469–489, https://doi.org/10.5194/tc-7-469-2013, 2013.

Fürst, J. J., Goelzer, H., and Huybrechts, P.: Ice-dynamic projections of the Greenland ice sheet in response to atmospheric and oceanic
5   warming, The Cryosphere, 9, 1039–1062, https://doi.org/10.5194/tcd-8-3851-2014, http://www.the-cryosphere-discuss.net/8/3851/2014/, 2015.

Goelzer, H., Huybrechts, P., Fürst, J., Nick, F., Andersen, M., Edwards, T., Fettweis, X., a.J. Payne, and Shannon, S.: Sensitivity of Greenland ice sheet projections to model formulations, Journal of Glaciology, 59, 733–749, https://doi.org/10.3189/2013JoG12J182, http://www.igsoc.org/journal/59/216/j12J182.html, 2013.

10 Helsen, M. M., van de Wal, R. S. W., van den Broeke, M. R., van de Berg, W. J., and Oerlemans, J.: Coupling of climate models and ice sheet models by surface mass balance gradients: application to the {Greenland} Ice Sheet, The Cryosphere, 6, 255–272, https://doi.org/doi:10.5194/tc-6-255-2012, 2012, 2012.

Inall, M. E., Murray, T., Cottier, F. R., Scharrer, K., and Boyd, T. J.: Oceanic heat delivery via Kangerdlugssuaq Fjord to the south-east Greenland ice sheet, Journal of Geophysical Research : Oceans, pp. 631–645, https://doi.org/10.1002/2013JC009295.Received, 2014.

15 Jackson, R. H., Straneo, F., and Sutherland, D. A.: Externally forced fluctuations in ocean temperature at Greenland glaciers in non-summer months, Nature Geoscience, 7, 503–508, https://doi.org/10.1038/ngeo2186, http://www.nature.com/ngeo/journal/v7/n7/full/ngeo2186.html?WT.ec{_}id=NGEO-201407, 2014.

Jackson, R. H., Shroyer, E. L., Nash, J. D., Sutherland, D. A., Carroll, D., Fried, M. J., Catania, G. A., Bartholomaus, T. C., and Stearns, L. A.: Near-glacier surveying of a subglacial discharge plume: implications for plume parameterizations, Geophysical Research Letters,
20   https://doi.org/10.1002/2017GL073602, http://doi.wiley.com/10.1002/2017GL073602, 2017.

Jenkins, A.: Convection-Driven Melting near the Grounding Lines of Ice Shelves and Tidewater Glaciers, Journal of Physical Oceanography, 41, 2279–2294, https://doi.org/10.1175/JPO-D-11-03.1, http://journals.ametsoc.org/doi/abs/10.1175/JPO-D-11-03.1, 2011.

Khan, S. a., Kjaer, K. H., Bevis, M., Bamber, J. L., Wahr, J., Kjeldsen, K. K., Bjork, A. a., Korsgaard, N. J., Stearns, L. a., van den Broeke, M. R., Liu, L., Larsen, N. K., and Muresan, I. S.: Sustained mass loss of the northeast Greenland ice sheet triggered by regional
25   warming, Nature Clim. Change, 4, 292–299, https://doi.org/10.1038/nclimate2161, http://dx.doi.org/10.1038/nclimate2161{%}5Cn10.1038/nclimate2161{%}5Cnhttp://www.nature.com/nclimate/journal/v4/n4/abs/nclimate2161.html{#}supplementary-information, 2014.

Moon, T., Joughin, I., Smith, B., and Howat, I.: 21st-Century Evolution of Greenland Outlet Glacier Velocities, Science, 336, 576–578, 2012.

Morlighem, M., Rignot, E., Mouginot, J., Seroussi, H., and Larour, E.: Deeply incised submarine glacial valleys beneath the Greenland ice sheet, Nature Geoscience, 7, 418–422, https://doi.org/10.1038/ngeo2167, http://www.nature.com/doifinder/10.1038/ngeo2167, 2014.

30 Mortensen, J., Bendtsen, J., Motyka, R. J., Lennert, K., Truffer, M., Fahnestock, M., and Rysgaard, S.: On the seasonal freshwater stratification in the proximity of fast-flowing tidewater outlet glaciers in a sub-Arctic sill fjord, Journal of Geophysical Research: Oceans, 118, 1382–1395, https://doi.org/10.1002/jgrc.20134, 2013.

Nick, F. M., Vieli, A., Andersen, M. L., Joughin, I., Payne, A., Edwards, T. L., Pattyn, F., and van de Wal, R. S. W.: Future sea-level rise from Greenland's main outlet glaciers in a warming climate, Nature, 497, 235–238, https://doi.org/10.1038/nature12068, http://www.nature.
35   com/doifinder/10.1038/nature12068, 2013.

Rignot, E. and Mouginot, J.: Ice flow in Greenland for the International Polar Year 2008-2009, Geophys. Res. Lett., 39, L11 501, https://doi.org/10.1029/2012GL051634, 2012.

Rignot, E., Box, J. E., Burgess, E., and Hanna, E.: Mass balance of the {Greenland} ice sheet from 1958 to 2007, Geophys. Res. Lett., 35, L20 502, https://doi.org/10.1029/2008GL035417, 2008.

Rignot, E., Fenty, I., Xu, Y., Cai, C., Velicogna, I., Cofaigh, C., Dowdeswell, J. A., Weinrebe, W., Catania, G., and Duncan, D.: Bathymetry data reveal glaciers vulnerable to ice-ocean interaction in Uummannaq and Vaigat glacial fjords, west Greenland, Geophysical Research Letters, 43, 2667–2674, https://doi.org/10.1002/2016GL067832, 2016.

Schaffer, J., Timmermann, R., Erik Arndt, J., Savstrup Kristensen, S., Mayer, C., Morlighem, M., and Steinhage, D.: A global, high-resolution data set of ice sheet topography, cavity geometry, and ocean bathymetry, Earth System Science Data, 8, 543–557, https://doi.org/10.5194/essd-8-543-2016, 2016.

Schaffer, J., von Appen, W. J., Dodd, P. A., Hofstede, C., Mayer, C., de Steur, L., and Kanzow, T.: Warm water pathways toward Nioghalvfjerdsfjorden Glacier, Northeast Greenland, Journal of Geophysical Research: Oceans, 122, 4004–4020, https://doi.org/10.1002/2016JC012462, 2017.

Sciascia, R., Straneo, F., Cenedese, C., and Heimbach, P.: Seasonal variability of submarine melt rate and circulation in an East Greenland fjord, Journal of Geophysical Research: Oceans, 118, 2492–2506, https://doi.org/10.1002/jgrc.20142, http://doi.wiley.com/10.1002/jgrc.20142, 2013.

Slater, D., Nienow, P., Sole, A., Cowton, T. O. M., Mottram, R., Langen, P., and Mair, D.: Spatially distributed runoff at the grounding line of a large Greenlandic tidewater glacier inferred from plume modelling, Journal of Glaciology, pp. 1–15, https://doi.org/10.1017/jog.2016.139, 2017.

Slater, D. A., Nienow, P. W., Cowton, T. R., Goldberg, D. N., and Sole, A. J.: Effect of near-terminus subglacial hydrology on tidewater glacier submarine melt rates, Geophysical Research Letters, 42, 2861–2868, https://doi.org/10.1002/2014GL062494, 2015.

Straneo, F. and Heimbach, P.: North Atlantic warming and the retreat of Greenland's outlet glaciers., Nature, 504, 36–43, https://doi.org/10.1038/nature12854, http://www.ncbi.nlm.nih.gov/pubmed/24305146, 2013.

Straneo, F., Sutherland, D. a., Holland, D., Gladish, C., Hamilton, G. S., Johnson, H. L., Rignot, E., Xu, Y., and Koppes, M.: Characteristics of ocean waters reaching greenland's glaciers, Annals of Glaciology, 53, 202–210, https://doi.org/10.3189/2012AoG60A059, 2012.

Syvitski, J., Andrews, J., and Dowdeswell, J.: Sediment deposition in an iceberg-dominated glacimarine environment, East Greenland: basin fill implications, Global and Planetary Change, 12, 251–270, https://doi.org/10.1016/0921-8181(95)00023-2, 1996.

van den Broeke, M., Box, J., Fettweis, X., Hanna, E., Noël, B., Tedesco, M., van As, D., van de Berg, W. J., and van Kampenhout, L.: Greenland Ice Sheet Surface Mass Loss: Recent Developments in Observation and Modeling, Current Climate Change Reports, 3, 345–356, https://doi.org/10.1007/s40641-017-0084-8, http://link.springer.com/10.1007/s40641-017-0084-8, 2017.

Xie, J., Bertino, L., Knut, L., and Sakov, P.: Quality assessment of the TOPAZ4 reanalysis in the Arctic over the period 1991-2013, Ocean Science, 13, 123–144, https://doi.org/10.5194/os-13-123-2017, 2017.

Xu, Y., Rignot, E., Fenty, I., Menemenlis, D., and Flexas, M. M.: Subaqueous melting of Store Glacier, west Greenland from three-dimensional, high-resolution numerical modeling and ocean observations, Geophysical Research Letters, 40, 4648–4653, https://doi.org/10.1002/grl.50825, http://doi.wiley.com/10.1002/grl.50825, 2013.
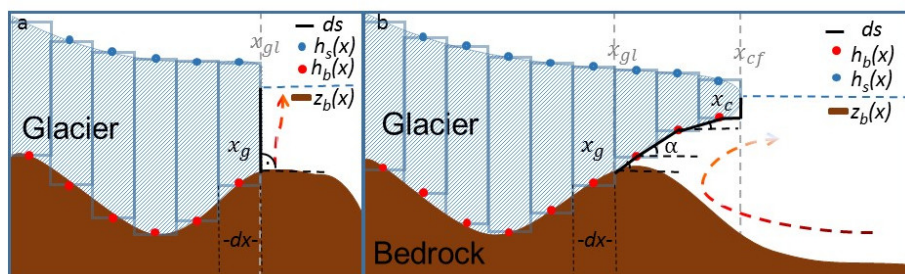
Figure 1. Visualiszation of 1D glacier model with the staggered grid for a) a tidewater glacier and b) a glacier with floating tongue. Red dots indicate where the values of glacier bottom h_b are defined and blue dots where surface elevation h_s of the glacier is defined. They are calculated at dx/2 - the half width of each grid cell. Last grounded cell has the coordinate x_g and last floating cell has the coordinate x_c. The grounding line gl_x is determined at the border of the last grounded cell, where the flotation criterion is not yet achieved. After the grounding line, the calculation of submarine melt along the distance ds (thick, black line) is performed with the line plume model. For a floating tongue (b) every grid cell may have a different angle for ds while for a tidewater glacier (a) the angle is set to 90 degrees. The bedrock elevation z_b (brown, thick line) is equal to h_b for the grounded part and is deeper for the floating part of the glacier.
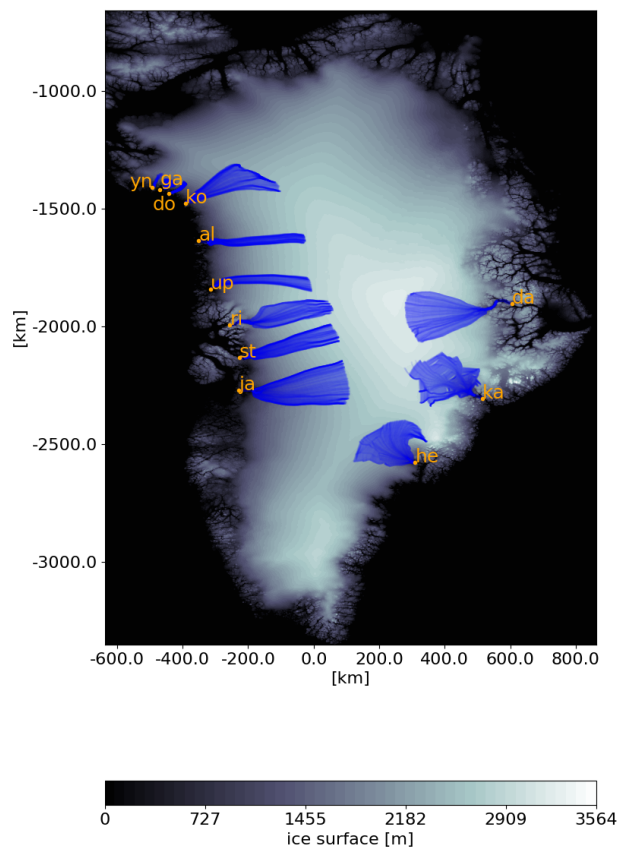
Figure 2. Terminus location (orange dot) with the catchment area (blue) of the twelve investigated glaciers: Alison Glacier (al), Daugaard-Jensen Glacier (da), Docker-Smith Glacier (do), Gade (ga) Helheim Glacier (he), Jakobshavn-Isbrae (ja), Kangerlussuaq Glacier (ka), Kong-Oscar Glacier (ko), Rink-Isbrae (ri), Store Glacier (st), Upernavik North Glacier (up), Yngvar-Nielsen Glacier (yn)
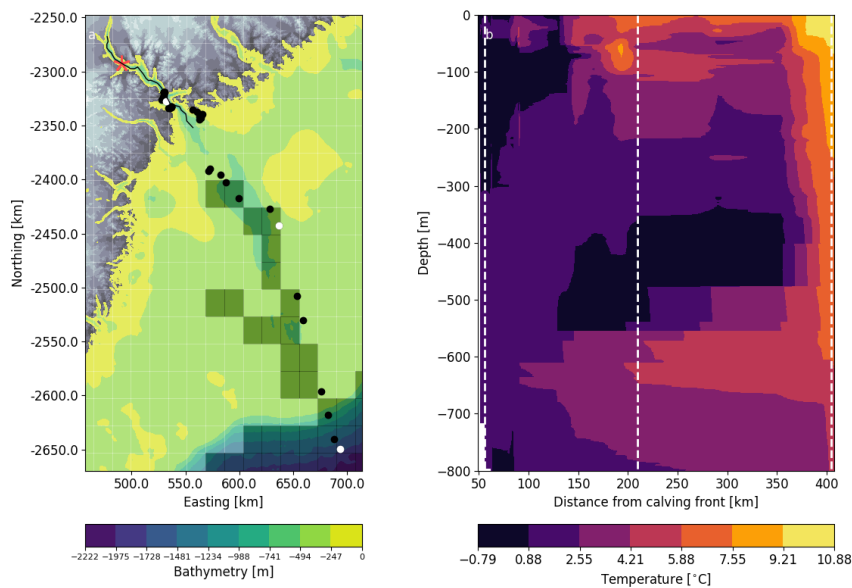
Figure 3. a) Bathymetry around Kangerlussuaq glacier (red star indicates glacier terminus). Black dots indicate the location of the CTD measurements in made September 2004. White dots show the location of CTD profiles used for the melt rate calculations. Grid indicates the resolution of the reanalysis data and grey shaded squares show which reanalysis data points have a minimum depth of 400m. b) Vertical temperature distribution as a function of the distance from the glacier terminus, obtained by interpolation od the CTD profiles. White dashed lines correspond to the position of the white-marked CTD positions in panel a.
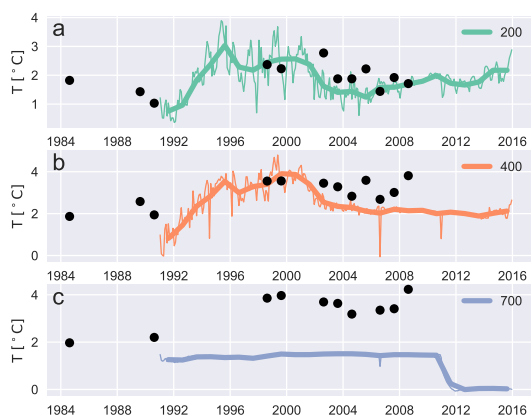
Figure 4. Monthly (thin lines) and annual mean (thick lines) of ocean temperature from reanalysis data of the closest point to fjord of Jakobshavn-Isbrae that has a minimum depth of a) 200m b) 400m and c) 700m depth. Location of these points differ due to the different area coverages for the corresponding depths (700m is mostly outside of continental shelf). Black dots show CTD measurements at the same depth but inside or close to the fjord.
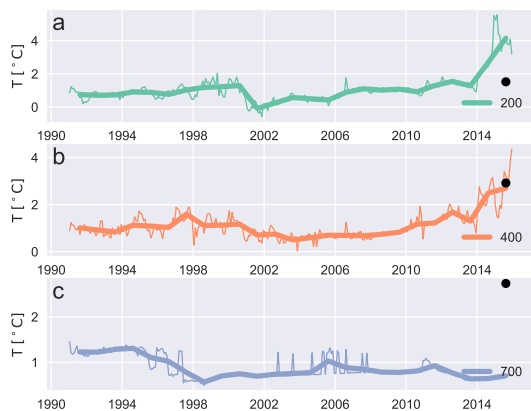
Figure 5. Same as in Fig. 4 but for Store Glacier.
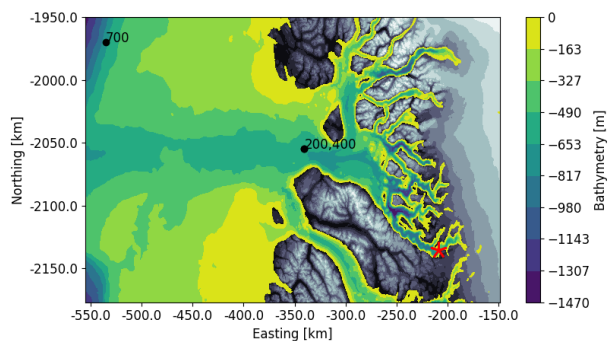
Figure 6. Bathymetry and bedrock data close to the terminus of Store Glacier (red star). The labels 200, 400 and 700 indicate were the detection points of the reanalysis data closest to the glacier with the depth of 200 m, 400 m and 700 m were located.
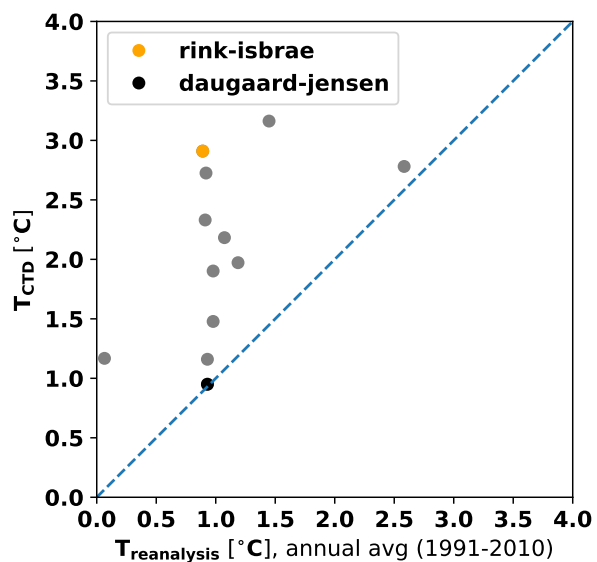
Figure 7. Depth-averaged temperature of CTD measurements closest to glacier front, inside the fjords (y-axis) and Reanalysis data of extrapolated 400m-depth points, averaged from 1991 -2010 (x-axis) for all 12 glaciers.
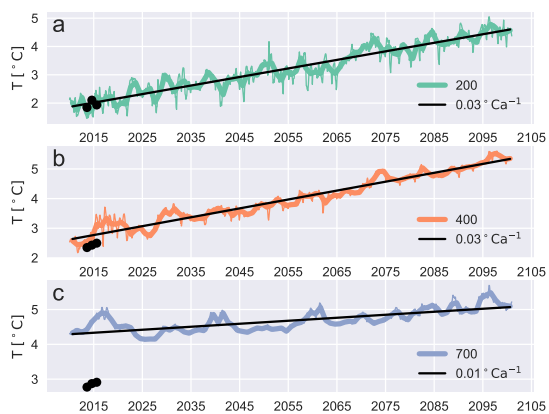
Figure 8. Monthly ocean temperature and centennial trend from the CMIP5 model MPI-ESM-LR in the closest points to the fjord of Rink Isbrae that have a model depth of at least a) 200m b) 400m and c) 700m depth. Black dots show CTD measurements at the same depth but inside the fjord.
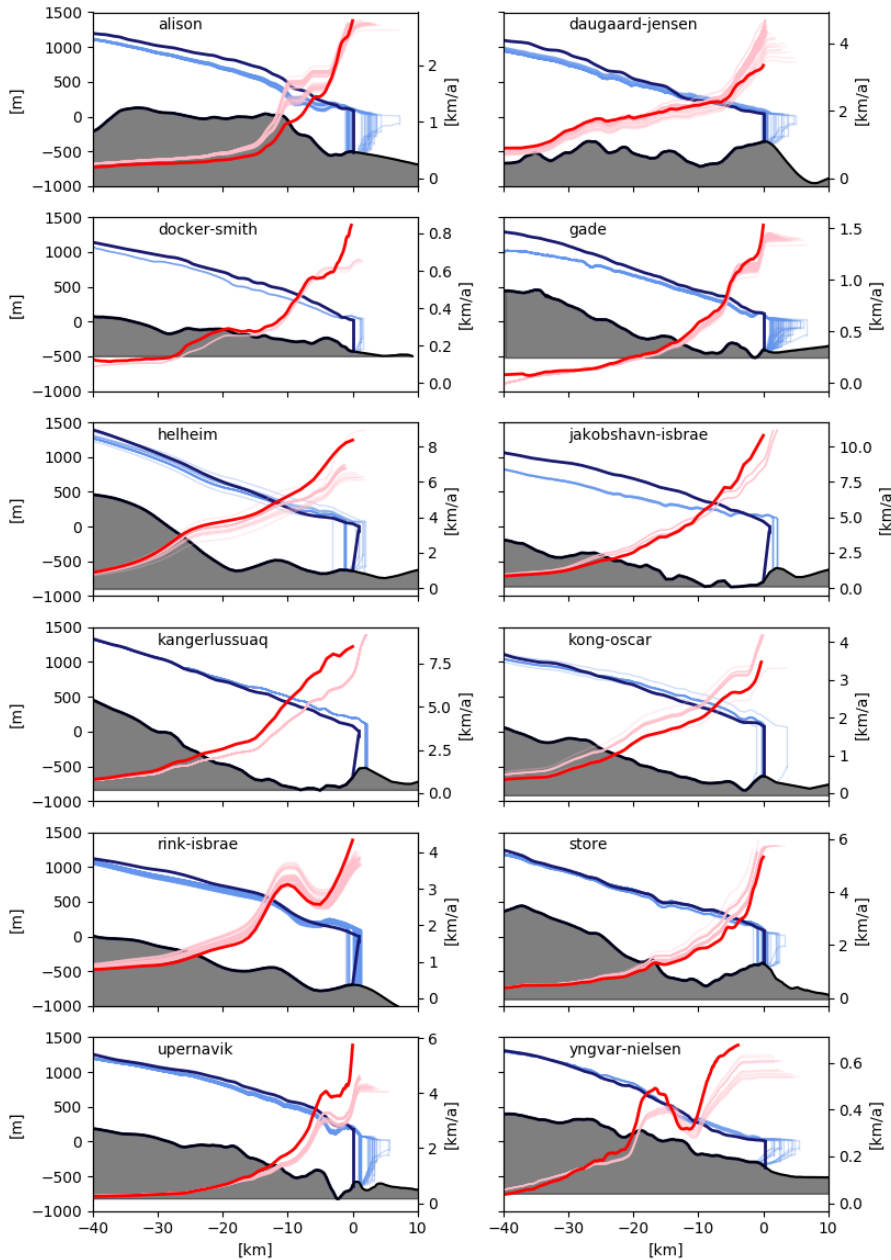
Figure 9. Glacier thickness (thick, blue) and velocity profile (thick, red) for the last 40 km to the grounding line from the derived geometry of the dataset published by Morlighem et al. (2014) and Rignot and Mouginot (2012).The resulting profiles of all stable states simulated by the line-plume glacier-flowline model are depicted in transparent lines.
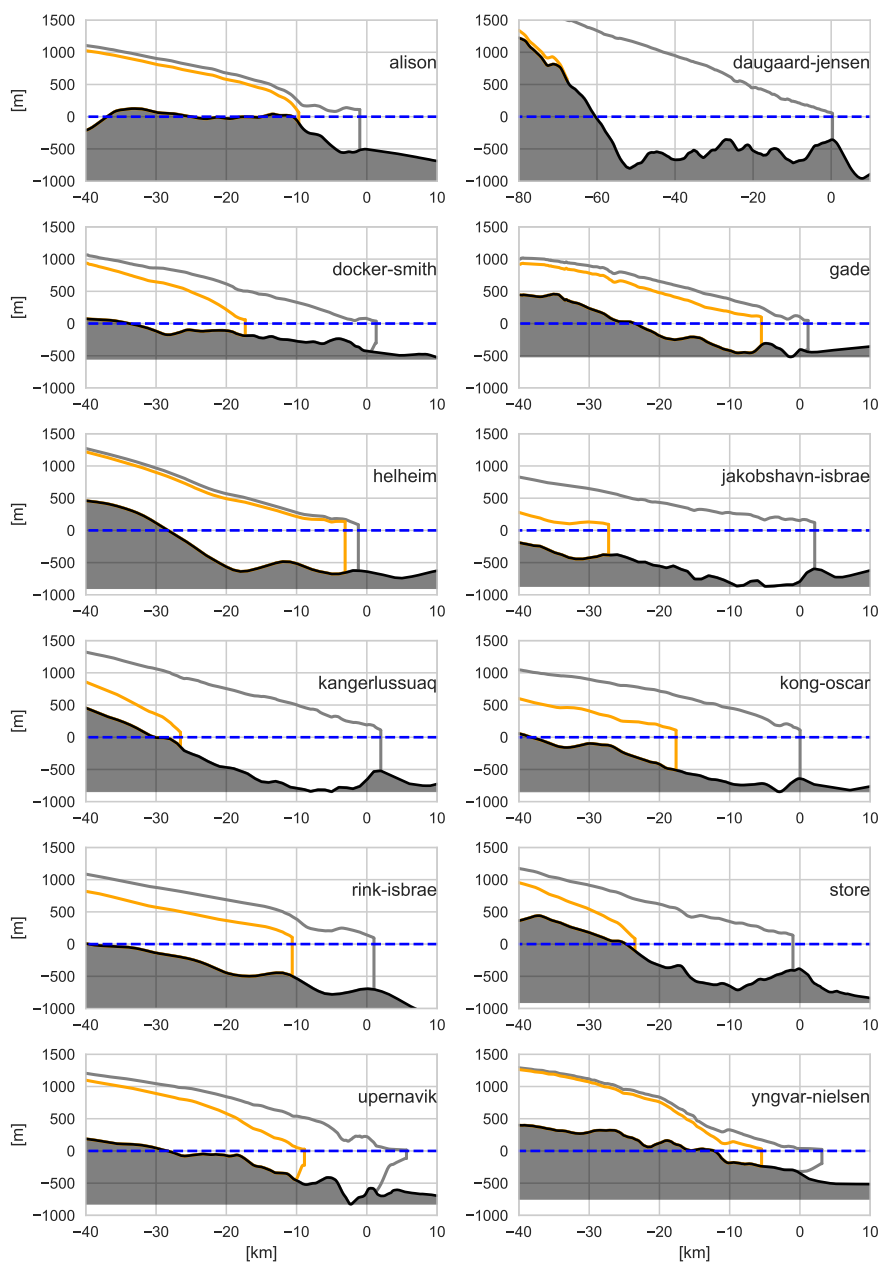
Figure 10. Retreat of median-range[3] SLR scenario for RCP 8.5 forcing scenarios (SMB and ocean temperature and subglacial discharge) for all 12 glaciers at 2100 (orange). Corresponding initial states are depicted in grey. Daugaard-Jensen, showed full retreat with over 80 km.
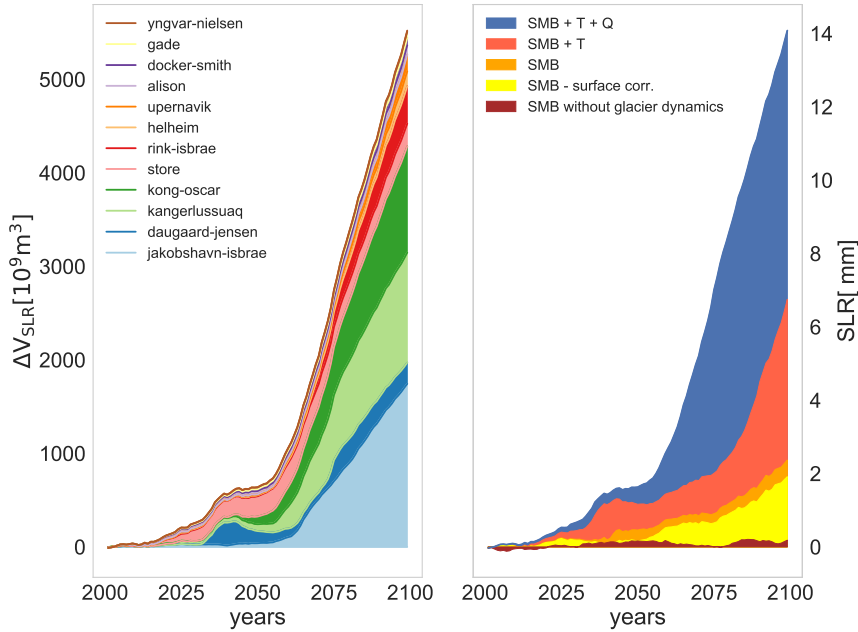
Figure 11. Cumulative sea level rise of median-range[3] SLR scenario from Fig. 10 for all 12 glaciers. The glaciers' response to complete future forcing scenario (smb, subglacial discharge Q and ocean temperature T in blue), without subglacial discharge forcing (SMB + T; pink), with SMB forcing only (orange) and excluding the surface elevation feedback (SMB, no dz; yellow). The SMB forcing vom MAR is calculated over the whole present-day catchment area of all glaciers (brown).
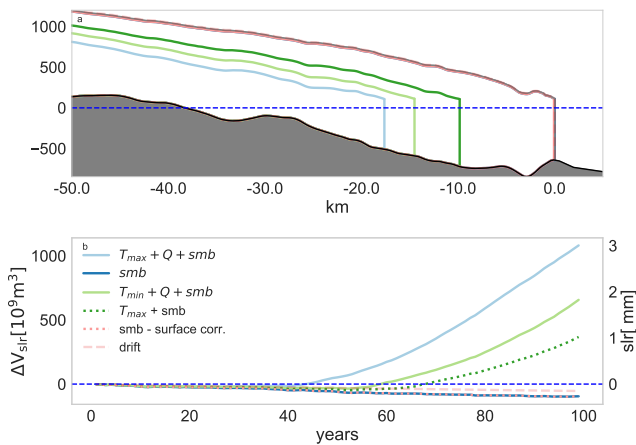
Figure 12. a) Kong-Oscar Glacier with a representative medium-slr retreat scenario applying forcing factors as subglacial discharge Q, ocean temperature T, surface mass balance smb with and without accounting for surface elevation correction (smb - surface corr.) for the medium SLR scenario. The corresponding SLR of each experiment is displayed in panel b).
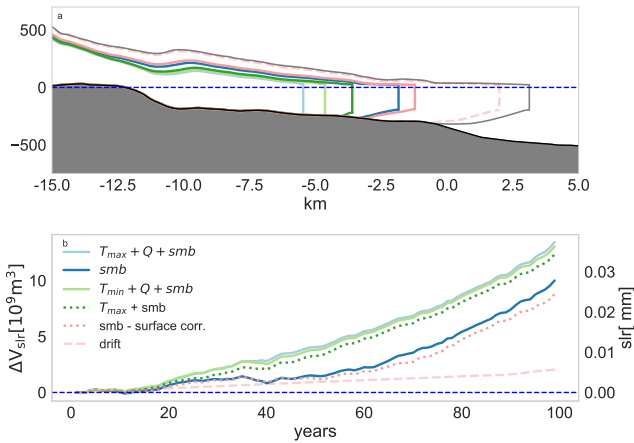
Figure 13. Same as 12 for the medium SLR scenario but for Yngvar Nielsen Glacier.
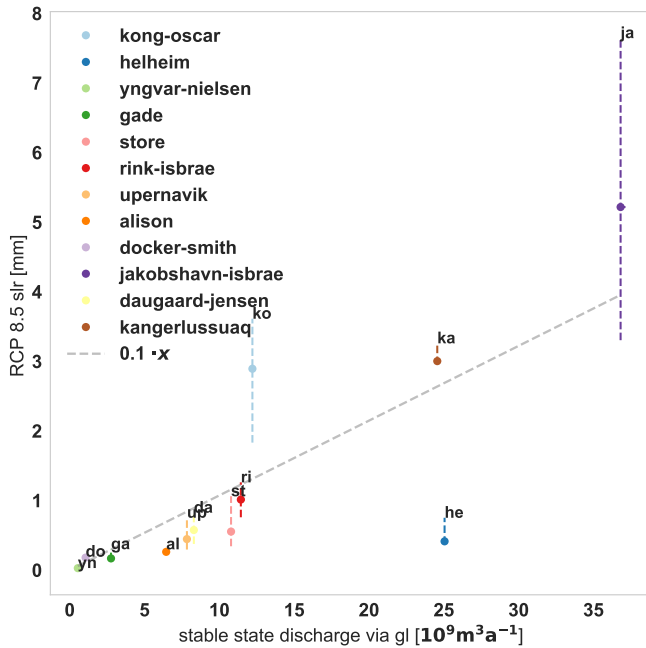
Figure 14. First to third quartile (median indicated with a dot) of contribution to SLR under RCP 8.5 for each glacier from Table 3 as a function of the present-day grounding line discharge. The future simulations were forced by changes in SMB, subglacial discharge and minimal and maximal ocean temperature trend 1. Grey dashed line, indicates a linear function of the present-day grounding line discharge in future SLR for 2100 obtained with an ordinary least square model from the median values. Slope and p-value are $0.1 \, \mathrm{mm \, km^{-3}}$ a and 0.27, respectively. The correlation is weak with a correlation coefficient with 0.35.
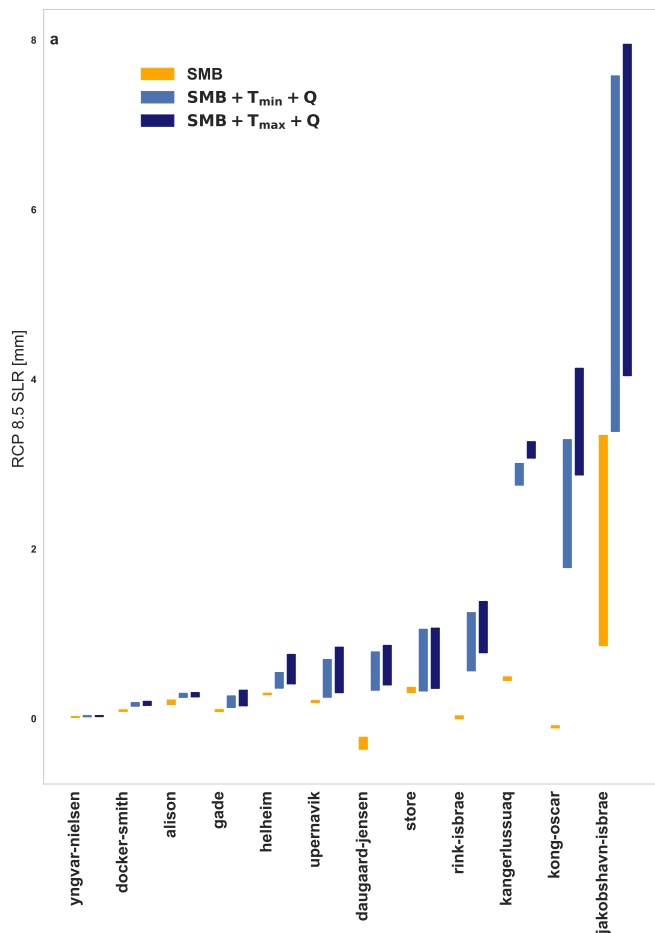
Figure 15. First to third quartile of contribution to SLR for each glacier. Future RCP 8.5 scenarios were either forced with SMB changes only (orange) or changes in SMB, ocean temperature ($T_{\min}$ and $T_{\max}$) and subglacial discharge (blue).

Table 1. Minimal and maximal ocean temperature trend derived by three CMIP5 Models close to each glacier fjord at 400m depth. Detailed information are listed in table S1.

glacier name	$\Delta T_{\min}(°C/100a)$	$\Delta T_{\max}(°C/100a)$
Daugaard-Jensen	3	5
Helheim Glacier	2	3
Jakobshavn Isbae	2	4
Kangerlussuaq Glacier	3	4
Rink Isbrae	1	3
Store Glacier	1	3
Kong Oscar Glacier	1	3
Alison Glacier	1	3
Upernavik Isstrom	1	3
Yngvar Nielsen	1	3
Docker Smith Glacier	1	3
Gade Glacier	1	3

Table 2. Each investigated glacier with the mean grounding line discharge from observation $\text{Flx}_{\text{gl}}^{\star\text{E}}$ (Enderlin and Howat, 2013) and from the stable state simulations Flx_{gl}. The melt flux range for floating termini from all present-day simulations MeltFlx and from the observational data $\text{MeltFlx}^{\star\text{E}}$ is calculated with the error ranges in Enderlin and Howat (2013) but with the condition $0 < \text{MeltFlx}^{\star\text{E}} < \text{Flx}_{\text{gl}}^{\star\text{E}}$. The respective ratio of melt flux /grounding line discharge in % is listed in the last to columns. Glaciers with $\star$ indicate were the melt rate partition of the simulation does not overlap with the error range of Enderlin and Howat (2013). Melt fluxes of are for floating tongue and thus $\text{MeltFlx} = 0$ indicates tidewater glaciers. Store Glacier is not examined in Enderlin and Howat (2013).

glacier	$\text{Flx}_{\text{gl}}^{\star\text{E}}$ 10^9 [m³/a]	Flx_{gl} 10^9 [m³/a]	$\text{MeltFlx}^{\star\text{E}}$ 10^9 [m³/a]	MeltFlx 10^9 [m³/a]	$\text{MeltFlx}^{\star\text{E}}/\text{Flx}_{\text{gl}}^{\star\text{E}}$ [%]	$\text{MeltFlx}/\text{Flx}_{\text{gl}}$ [%]
Alison	6.83	6.25 - 6.55	0.82 - 6.41	0.00 - 4.77	12 - 94	0 - 76
Daugaard-Jensen	9.34	7.36 - 8.45	4.12 - 9.34	0.00 - 5.26	44 - 100	0 - 69
Docker-Smith	1.06	1.05 - 1.07	0.00 - 0.87	0.22 - 0.66	0 - 82	20 - 62
Gade	4.85	2.63 - 2.81	0.00 - 4.85	0.16 - 2.14	0 - 100	6 - 77
Helheim	29.16	20.94 - 25.94	0.19 - 6.90	0.00 - 8.39	1 - 24	0 - 36
Jakobshavn Isbrae*	43.03	36.81 - 37.14	21.11 - 32.91	0.00 - 0.00	49 - 76	0 - 0
Kangerlussuaq	38.80	24.51 - 24.58	0.00 - 6.83	0.00 - 0.00	0 - 18	0 - 0
Kong-Oscar	11.86	10.34 - 12.86	3.06 - 6.28	0.00 - 2.64	26 - 53	0 - 26
Rink-Isbrae	10.95	11.20 - 12.25	0.00 - 6.85	0.00 - 0.00	0 - 63	0 - 0
Store	-	10.54 - 11.31	-	0.00 - 8.38	-	0 - 77
Upernavik North	17.12	7.48 - 7.87	5.81 - 11.20	0.03 - 5.92	34 - 65	0 - 78
Yngvar Nielsen	0.69	0.53 - 0.57	0.00 - 0.69	0.08 - 0.42	0 - 100	15 - 76

Table 3. Median, first and third quartile of SLR contribution from each glacier under RCP 8.5 (smb, subglacial discharge and ocean temperature (min and max)). Values are corrected from drift. Negative values in SLR indicate smb gain.

glacier	slr [mm]		
	median	first quartile	third quartile
Alison	0.26	0.26	0.30
Daugaard-Jensen	0.58	0.38	0.83
Docker-Smith	0.18	0.15	0.19
Gade	0.17	0.14	0.30
Helheim	0.41	0.38	0.85
Kangerlussuaq	3.00	2.96	3.26
Kong-Oscar	2.89	1.83	3.61
Rink Isbrae	1.01	0.76	1.26
Store	0.62	0.38	1.10
Upernavik	0.45	0.30	0.76
Yngvar-Nielsen	0.03	0.03	0.03
Jakobshavn Isbrae	5.22	3.30	7.65
sum	14.83	10.88	20.14

Table 4. Median, first and third quartile of grounding line retreat from each glacier under RCP 8.5 (smb, subglacial discharge and ocean temperature (min and max)). Values are corrected from drift.

	groundling line retreat [km]		
glacier	median	first quartile	third quartile
alison	9.17	8.69	10.77
daugaard-jensen	39.26	30.88	39.78
docker-smith	15.13	14.23	16.49
gade	5.85	4.62	15.17
helheim	1.52	1.10	9.63
kangerlussuaq	28.52	28.44	28.53
kong-oscar	17.65	14.61	18.63
rink-isbrae	11.00	10.63	11.15
store	10.02	1.97	22.77
upernavik	6.91	2.68	16.32
yngvar-nielsen	4.69	4.28	5.22
jakobshavn-isbrae	38.57	19.85	40.53
sum	188.28	142.00	235.00